In situ analysis of garnet inclusion in diamond using single-crystal X-ray diffraction and X-ray micro-tomography

Fabrizio NESTOLA[1,2,*], Marcello MERLI[3], Paolo NIMIS[1,2], Matteo PARISATTO[1], Maya KOPYLOVA[4], Andrea DE STEFANO[4], Micaela LONGO[1], Luca ZIBERNA[1] and Murli MANGHNANI[5]

[1] Department of Geosciences, Università degli Studi di Padova, Via Gradenigo 6, 35131 Padova, Italy
[2] IGG-CNR, UO Padova, Via Gradenigo 6, 35131 Padova, Italy
*Corresponding author, e-mail: fabrizio.nestola@unipd.it
[3] Dipartimento CFTA, Università di Palermo, Via Archirafi 36, 90126 Palermo, Italy
[4] Department of Earth and Ocean Sciences, The University of British Columbia, Vancouver, BC, Canada V6T 1Z4
[5] Hawaii Institute of Geophysics and Planetology, University of Hawaii, 1680 East-West Road, Honolulu, HI, USA

Abstract: A single crystal of garnet enclosed in a diamond from the Jericho kimberlite (Slave Craton, Canada) has been investigated using X-ray diffraction and X-ray micro-tomography. The novel experimental approach allowed us to determine the crystal structure of the garnet. The unit-cell edge a and fractional atomic coordinates of oxygen were used to determine the composition via an updated Margules model for garnets. The composition is $Pyr_{0.41(5)}Alm_{0.36(7)}Gro_{0.22(1)}Uva_{0.01(1)}$, which is indistinguishable from the eclogitic garnets found in other Jericho diamonds. We also demonstrated that residual pressures on the inclusion of up to 1 GPa do not affect significantly the determination of the garnet composition by structure refinement.

Key-words: diamond, garnet, inclusion, residual pressure, X-ray diffraction, X-ray micro-tomography, Jericho kimberlite.

1. Introduction

The study of mineral inclusions in diamonds is providing invaluable insight into the geochemistry, geodynamics and geophysics of the Earth's mantle. Studying diamond inclusions, which are the only ultra-deep samples we have of the Earth, allows the $P\text{-}T\text{-}fO_2$ conditions and timing of diamond formation to be evaluated. However, *in situ* investigation of the inclusions using non-destructive techniques remains challenging. Together with micro-Raman spectroscopy (Barron *et al.*, 2008 and references therein) and transmission X-ray diffraction (Smith *et al.*, 2011), one of the potentially most powerful non-destructive methods is single-crystal X-ray diffraction. The main advantage of the diffraction technique is its unique capability to provide unit-cell parameters and crystal structure information. However, the application of such technique to mineral inclusions is hampered by the difficulty of centring the inclusion in the X-ray beam (*e.g.*, Kunz *et al.*, 2002). Because of this fundamental experimental problem, normally only unit-cell parameters have been previously obtained for the inclusions. Recently, crystal structure data have been reported for the first time for *in situ* inclusions (Nestola *et al.*, 2011; Joswig, 2011). Knowing both the unit-cell parameters and the crystal structure of an inclusion, it is possible to evaluate the remnant pressure

on the inclusion, which can then be related to the pressure of formation (*e.g.*, Nestola *et al.*, 2011), and to derive the mean number of electrons at each crystallographic site, from which chemical information can be indirectly extracted. The *in situ* determination of the composition of an inclusion is relatively straightforward for phases such as olivine, orthopyroxene, ringwoodite, and ferropericlase, which show very limited cation substitution (essentially only Mg/Fe substitution). For chemically more complex phases such as garnet and clinopyroxene, which are among the most abundant minerals included in diamonds (*cf.* Stachel & Harris, 2008, and references therein), the determination of composition is much more challenging.

To our knowledge, the only direct chemical analysis of inclusions still trapped in diamond have been thus far been obtained on a single diamond by micro X-ray fluorescence using synchrotron radiation (Brenker *et al.*, 2005). The reported absolute uncertainties in the Ca contents of Ca-silicate minerals were ±5–6 wt%. So, this technique appears to be more useful for mineral identification rather than for full chemical analysis (Sitepu *et al.*, 2005). More recently, Yasuzuka *et al.* (2009) proposed a method to estimate the Mg# value [$= 100 \cdot Mg_{mol}/(Mg + Fe)_{mol}$] of olivine inclusions from their Raman spectra with an uncertainty of ±0.8. In both cases, the errors in the resulting major-element data were much larger than in

conventional electron microprobe analyses, *i.e.*, much larger than generally required for detailed petrologic and thermobarometric studies. No data have been obtained so far on garnet inclusions enclosed in the host diamond. This mineral phase is often used to derive constraints on the origin and conditions of formation of the host diamond (*e.g.*, Stachel & Harris, 2008), but this is typically done using destructive techniques, which are required to expose the inclusion for conventional geochemical analysis.

In this work, we investigated a garnet inclusion of an unknown paragenesis (peridotitic, eclogitic or websteritic) fully enclosed in a diamond from the Jericho kimberlite (Slave Craton, Canada). We used an experimental approach that was extensively tested in crystallographic studies of single crystals loaded in diamond anvil cells (*e.g.*, Angel *et al.*, 1997, 2000; Nestola *et al.*, 2005, 2008) and was recently applied for the first time to the study of an olivine included in diamond (Nestola *et al.*, 2011). The inclusion we studied was barely visible under an optical microscope, being concealed under a frosted and resorbed surface of the diamond host (Fig. 1). The main aim of our study was to define the composition of the inclusion and the source assemblage of the host diamond using a completely non-destructive method, *i.e.*, without extracting the inclusion or cutting/polishing the diamond to allow its examination by conventional analytical methods.

Sample material and experimental techniques

The investigated diamond is a 0.001 carat sub-octahedral crystal extracted from the Jericho kimberlite (Slave Craton, Canada). Under the optical microscope only the largest inclusion is barely visible (see Fig. 1). The diamond and its inclusion content have been characterised by X-ray computed micro-tomography and single-crystal X-ray diffraction.

Fig. 1. Photomicrograph of the diamond studied in this work. The longest dimension of the diamond is about 0.5 mm.

X-ray computed micro-tomography (X-μCT)

X-ray computed micro-tomography (X-μCT) is an established technique for the microstructural investigation of many kinds of materials. It represents the evolution of the well-known computerized axial tomography (CAT) method, originally developed for medical purposes. X-μCT can provide, in a totally non-invasive manner, three-dimensional maps of the variations at the micrometric scale of the X-ray attenuation coefficient within a sample. The technique is based on the acquisition of a very large number of X-ray radiographs from different angular positions around a vertical rotation axis, followed by the application of a mathematical algorithm for the reconstruction of cross-sectional images called slices (*cf.* Kak & Slaney, 1988, for details). Such images can be stacked together to obtain a 3D digital model of the investigated object from which cross-sections or slices can be constructed by software in any desired orientation. In the reconstructed images, the grey values of the different phases are proportional to their attenuation coefficient (*i.e.*, black for air and voids, white for the most absorbing materials, such as iron-rich minerals).

In this work, an X-μCT scan of the investigated diamond was carried out in order to (i) check for the presence of mineral inclusions, tentatively detected by optical examination, (ii) determine the position and crystal size of the inclusion(s) with a spatial resolution of a few micrometres, and (iii) aid subsequent centring of the investigated inclusion under the X-ray beam of the single-crystal diffractometer, thus avoiding the need for several time-consuming preliminary X-ray scans (*cf.* Nestola *et al.*, 2011). The measurement was carried out at the Department of Geosciences of the University of Padova, using a SkyScan 1172 high-resolution X-μCT scanner. The system was equipped with a polychromatic microfocus X-ray tube, characterised by a maximum operating voltage of 100 kV and a maximum output power of 10 W. The anode material was tungsten and the focal spot size approximately 5 μm. The raw data (radiographs) were collected by a high-resolution 12-bit detection system, consisting of a scintillator screen (4000 × 2672 pixels, ~ 9 μm pixel size) coupled to a CCD chip by a tapered fibre-optic bundle. Due to the cone-beam geometry of the source, the image resolution can be adjusted according to the size of the specimen by simply varying the source-detector and source-object distances (D_{sd} and D_{so}); the ratio D_{sd}/D_{so} represents the geometrical magnification factor.

During data acquisition, the tube voltage and current were set to 40 kV and 250 μA, respectively. A total of 1200 absorption radiographs were acquired over a 360° rotation with an angular step of 0.3° between each exposure, with an exposure time per frame of 4.3 s. A 0.5 mm-thick aluminium filter was placed in the beam path in order to suppress the low-energy portion of the spectrum and minimize undesired artefacts related to the ''beam-hardening'' effect (*i.e.*, the preferential attenuation of low-energy X-rays while passing through the sample). A magnification factor of 6.55 was selected for the experiment,

resulting in a nominal spatial resolution for the resulting model of 1.36 µm. The reconstruction of cross-sectional slices from the acquired 2D projections was carried out using a modified FDK algorithm (Feldkamp *et al.*, 1984) for cone-beam geometry implemented in the SkyScan NRecon software; corrections for the beam-hardening effect and ring artefacts (*i.e.*, circular features due to anomalous responses of the detector, *cf.* Sijbers & Postnov, 2004) were also applied during the reconstruction process.

Single-crystal X-ray diffraction

The experimental approach used in this work is essentially the same as that adopted by Nestola *et al.* (2011) for their *in situ* crystallographic study of an olivine inclusion in diamond, and utilizes two four-circle single-crystal diffractometers. Unit-cell parameters of the largest inclusion detected by X-ray micro-tomography were determined by X-ray diffraction experiments on a STOE STADI IV four-circle diffractometer (installed at the Department of Geosciences, University of Padova) operating at 50 kV and 40 mA (Mo$K\alpha$ radiation), equipped with a point detector and controlled by the software SINGLE (Angel & Finger, 2011). This diffractometer was optimized for measurement of unit-cell parameters following recommendations in Angel *et al.* (2000). Preliminary centring of the crystal under the X-ray beam was obtained using the information from X-ray micro-tomography. Accurate centring was then achieved by iterative adjustment of the crystal offset calculated by the software SINGLE (Angel & Finger, 2011). During the centring procedure, the effects of crystal offsets and diffractometer aberrations were eliminated from the refined peak positions by the eight-position centring method of King & Finger (1979). Typical half-widths of the reflections were between 0.10 and 0.12° in ω. The variations among the half-widths for different reflections are within about 1σ. Unconstrained unit-cell parameters were obtained by vector least-squares centring (Ralph & Finger, 1982) of 18 diffraction maxima up to $2\theta_{max} = 30°$. The symmetry-constrained unit-cell parameters reported in Table 1 were found to be within one estimated standard deviation of the unconstrained ones.

The sample was then transferred along with its holder to a second four-circle STOE STADI IV diffractometer, equipped with a CCD detector from Oxford Diffraction, which allowed collection of complete intensity data. In this case, accurate centring of the crystal under the X-ray beam was achieved by allowing for the known geometrical relations between the two diffractometers. The data were acquired using Mo$K\alpha$ radiation from a sealed-tube source operated at 50 kV and 40 mA. A 1° ω-scan was used, collecting 570 frames with an exposure time of 15 s. The sample-detector distance was set to 60 mm. The collected dataset was limited to $2\theta \le 60°$ due to the high backgrounds in high-resolution data. The CrysAlis RED software (Oxford Diffraction) was used to integrate the intensity data, applying the Lorentz-polarization correction, while the X-RED (Stoe & Cie, 2001) and X-SHAPE

(Stoe & Cie, 1999) programs were used to correct for absorption due to the garnet crystal. Absorption due to the diamond host was not corrected for, because we estimate that the combination of small size, low linear absorption coefficient of diamond ($\mu = 0.20$ mm^{-1} for Mo$K\alpha$) and equant shape, the range of absorption due to the diamond is of the order of 5 %, which is probably less than the uncertainty in the calculation of transmission coefficient for an individual reflection from the garnet.

The reflections 0 0 8, 8 8 8, 2 2 12 and 2 8 12 were omitted from subsequent structure refinements because of the large discrepancies between observed and calculated structure intensities which we attributed to double diffraction effects. The structure refinement was performed in the $Ia\bar{3}d$ space group using the SHELXL software (Sheldrick, 2008). Ionic and neutral scattering factors were used for cations (Mg and Mg^{2+}, Fe and Fe^{2+}, Ca and Ca^{2+}, Al and Al^{3+}, Cr and Cr^{3+}, Si and Si^{4+}) and for oxygen (O and O^{2-}) as suggested in Merli *et al.* (1995).

Due to the low ratio of unique reflections with Fo > 4sig(Fo) to refined parameters, which is only 2.8 (*i.e.*, 76 unique reflections against 27 refined parameters) with anisotropic displacement parameters, we decided to refine the structure isotropically. The isotropic refinement has a better reflection/parameter ratio of 4.2 and the refinement quality is still satisfactory (see Table 1). The least-squares procedure using 188 unique reflections allowed us to obtain satisfactory agreement factors, $R_{obs} \sim 1.1$ % (76 reflections with $I/\sigma(I) > 2$) and $R_{all} \sim 7.3$ %, fully comparable with structure refinements of garnets not included in a diamond. It should be noted that, because of the high background of the diffraction patterns, the commonly adopted SHELXL weighting scheme results in unreasonably low values for the goodness of fit ($GooF_{obs}$) of less than 0.6. For this reason, a different weighting function was adopted, by manual setting of the parameters for the SHELXL WGHT keyword [$a = 0$, $b = 0$, $c = 5.0$, $d = 0$, $e = 0$, that yielded $w = \exp(5.0(\sin(\theta)/\lambda)^2)/\sigma^2(Fo^2)$]. Using this formula, the structure refinement gave a final $GooF_{obs} = 1.06$. The number of electrons obtained by the refinement at X and Y sites were 19.1(1.0) and 13.7(0.2), respectively, while the Z site was considered fully occupied by Si. The structure refinement details are reported in Table 1.

Table 1. Crystal structure refinement details for the garnet inclusion investigated in this work.

Unit-cell edge	11.5826 (2) Å
Unit-cell volume	1553.88 (5) Å^3
Z	8
Space group	$Ia\bar{3}d$
X-ray density	3.867 g/cm^3
Software	SHELXL-97
$2\theta_{max}$	60°
Unique reflections	188
$R_{2\sigma}$	1.06 %
R_{all}	7.03 %
GooF	1.06
Refined parameters	18
Extinction coefficient	0.00102 (15)

Results

X-ray micro-tomography

A single X-ray radiograph and the final 3D digital model of the investigated diamond are shown in Figs. 2 and 3, respectively. Owing to the high absorption contrast between diamond (highly transparent to X-rays) and the most common silicate mineral phases, some high-absorbing inclusions could be easily distinguished from the host crystal by simply thresholding the grey value histogram of the reconstructed images. Besides the large inclusion previously detected by optical examination and subsequently investigated by means of single-crystal XRD, six other smaller inclusions were identified. Among this set of smaller objects, only the largest one showed a mean grey value similar to the main inclusion, while the remaining ones appeared to be slightly less attenuating. For this reason, the inclusions were marked with two different colours in the 3D model of Fig. 3. However, it has to be pointed out that the observed difference in the mean grey values does not represent reliable evidence of the presence of two distinct mineral phases. In fact, owing to the use of a polychromatic X-ray source, the preferential attenuation of the low-energy portion of the spectrum while passing through dense objects may have led to an overestimation of the attenuation coefficient of the two largest inclusions during the reconstruction process. Such ambiguity cannot be resolved from the present data but could be overcome by using synchrotron-based X-μCT systems, which offer the major advantage of working with monochromatic radiation, thus avoiding ''beam hardening'' effects.

The inclusion studied in this work by means of single-crystal XRD corresponds to the largest absorbing feature
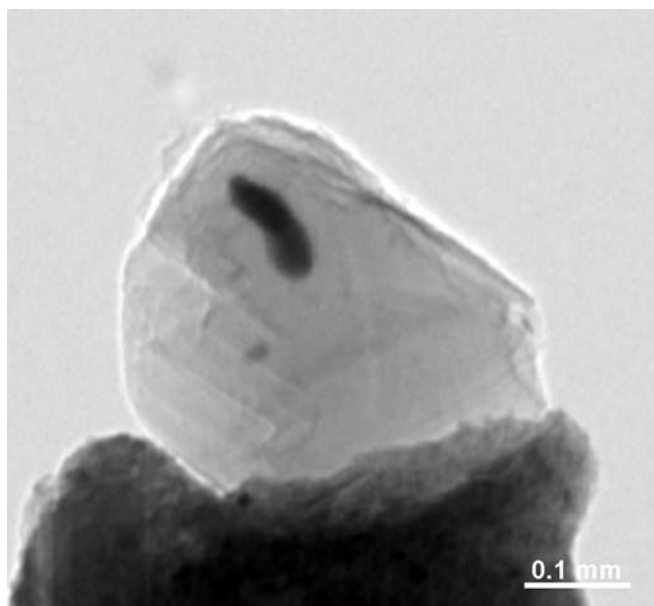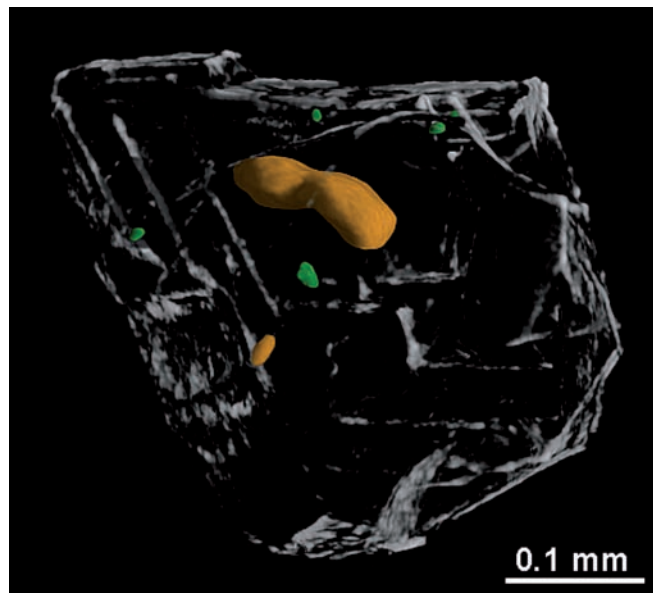
Fig. 3. Semi-transparent 3D reconstructed model of the investigated diamond showing the inclusions contained within it. The semi-transparency of the host diamond is made possible by edge enhancement effects related to phase contrast phenomena (Wilkins *et al.*, 1996) due to the deviation of the X-ray wave-fronts at the interface between diamond and air. The inclusions shown in orange colour are garnet crystals, whereas those shown in green inclusions are attributed to an unidentified phase with a lower X-ray absorption coefficient.

recognizable in the X-ray radiograph shown in Fig. 2. The shape of the inclusion is better illustrated in the 3D digital model reported in Fig. 3. Because of its elongated and kinked shape, one might surmise that the inclusion actually consists of two distinct inclusions very close to each other but this possibility was later refuted on the basis of X-ray diffraction data: in detail, 72 % of total were indexed with a single garnet orientation matrix, 20 % of total were indexed with a single diamond orientation matrix and 8 % remained unindexed.

The volume of the largest inclusion, having a maximum length of approximately 150 μm, was calculated using the ImageJ software (Abramoff *et al.*, 2004) and related plugins, and found to be 0.00052 mm^3. The maximum dimensions of the host diamond measured along three orthogonal axes were 410, 500 and 540 μm respectively.

Unit-cell edge, structure model and estimated garnet composition

X-ray diffraction data indicate that the investigated inclusion has cubic symmetry with a unit-cell edge $a = 11.5826(2)$ Å within the small measurement uncertainties. The fact that the unit-cell parameters exhibit cubic symmetry indicate that the inclusion is not subject to deviatoric stress. Therefore, the uniform slight broadening of the diffraction maxima compared to gem-quality crystals measured on the same instrument must arise from mosaic spread in the garnet inclusion.


Fig. 2. A single X-ray radiograph of the investigated sample (mounted on plasticine, shown as dark grey colour at the bottom part of the image). The inclusion investigated by XRD is the largest dark feature within the diamond, and some other smaller inclusions are also visible.

Based on the work by Merli *et al.* (1995), we present an updated automatic procedure for the determination of reliable garnet compositions starting from crystal-structure refinement data. The procedure is based on multiple regression equations for the independent estimates of the unit-cell edges and variable structural parameters (*i.e.*, the fractional coordinates of the oxygen atom) as a function of the cation content expressed in terms of garnet end-members. Based on the common compositions of garnets included in diamonds from the Jericho kimberlite (*cf.* De Stefano *et al.*, 2009), the end-members considered for the garnet investigated here were pyrope (PYR, $Mg_3Al_2Si_3O_{12}$), almandine (ALM, $Fe_3Al_2Si_3O_{12}$), grossular (GRO, $Ca_3Al_2Si_3O_{12}$) and uvarovite (UVA, $Ca_3Cr_2Si_3O_{12}$).

Relevant geometrical parameters (*i.e.*, the unit-cell edge *a* and fractional atomic coordinates of oxygen $x(O)$, $y(O)$, $z(O)$) were fitted using a model based on the classical Margules formalism, which takes into account the interaction between paired end-members. The following refined parameters were obtained by fitting up to 281 selected experimental data reported in Merli *et al.* (1995):

(1) K_{PYR}, K_{ALM}, K_{GRO}, K_{UVA} (linear coefficients for an ideal solid solution, following Vegard's law);

(2) W_{PYRALM}, W_{PYRGRO}, W_{GROALM}, W_{UVAPYR}, W_{UVAGRO}, (Margules interaction parameters for a regular symmetric solid solution);

(3) W_{PYR^2ALM}, W_{PYR^2GRO}, W_{ALM^2PYR}, W_{ALM^2GRO}, W_{GRO^2PYR}, W_{GRO^2ALM}, (Margules interaction parameters for a sub-regular asymmetric solid solution).

The general form of each predicting equation was thus: geometric parameter

$$
\begin{aligned}
= \ & K_{ALM} \cdot \chi_{ALM} + K_{GRO} \cdot \chi_{GRO} \\
& + K_{UVA} \cdot \chi_{UVA} + W_{PYRALM} \cdot \chi_{PYR}\,\chi_{ALM} \\
& + W_{PYRGRO} \cdot \chi_{PYR}\,\chi_{GRO} + W_{GROALM} \cdot \chi_{GRO}\chi_{ALM} \\
& + W_{UVAPYR} \cdot \chi_{UVA}\chi_{PYR} + W_{UVAGRO} \cdot \chi_{UVA}\,\chi_{GRO} + \\
& + W_{PYR^2ALM} \cdot \chi_{PYR}{}^2\chi_{ALM} + W_{ALM^2PYR} \cdot \chi_{ALM}{}^2\chi_{PYR} + \\
& + W_{PYR^2GRO} \cdot \chi_{PYR}{}^2\chi_{GRO} + W_{GRO^2PYR} \cdot \chi_{GRO}{}^2\chi_{PYR} \\
& + W_{ALM^2GRO} \cdot \chi_{ALM}{}^2\chi_{GRO} + W_{GRO^2ALM} \cdot \chi_{GRO}{}^2\chi_{ALM} \\
& + (\text{geometrical parameter})_{PYR}
\end{aligned}
$$

where "geometric parameter" can be *a*, $x(O)$, $y(O)$, or $z(O)$, and χ_i is the mole fraction of the end-member *i*. Note that the interaction Margules parameters involving uvarovite have been limited to those of a regular symmetric solid solution. More complicated models taking into account three- or four-component mixing terms have been rejected because of the difficulty in obtaining statistically reliable parameter estimates. This fact may be ascribed to the strong correlations between the parameters to be refined.

The resulting equations, which express each geometric parameter as a function of the molar fractions χ of each end-member are:

$$
\begin{aligned}
a(\text{Å}) =\ & 0.070443\chi_{ALM} + 0.398956\chi_{GRO} + 0.314779\chi_{UVA} \\
& + {-0.331507}\chi_{PYR}\chi_{ALM} + 0.481939\chi_{PYR}\chi_{GRO} \\
& - 0.121610\chi_{GRO}\chi_{ALM} + {+0.341464}\chi_{UVA}\chi_{PYR} \\
& + 0.382305\chi_{UVA}\chi_{ALM} + 2.353796\chi_{UVA}\chi_{GRO} \\
& + {+0.332479}\chi_{PYR}{}^2\chi_{ALM} - 0.431806\chi_{PYR}{}^2\chi_{GRO} \\
& + 0.387444\chi_{ALM}{}^2\chi_{PYR} + {+0.125574}\chi_{ALM}{}^2\chi_{GRO} \\
& - 0.390760\chi_{GRO}{}^2\chi_{PYR} + 0.205330\chi_{GRO}{}^2\chi_{ALM} \\
& + {+11.451443} \pm 0.0035
\end{aligned} \tag{1}
$$

$$
\begin{aligned}
x(O) =\ & 0.001160\chi_{ALM} + 0.005338\chi_{GRO} - 0.009234\chi_{UVA} \\
& + {+0.003138}\chi_{PYR}\chi_{ALM} + 0.003193\chi_{PYR}\chi_{GRO} \\
& - 0.007504\chi_{GRO}\chi_{ALM} + {-0.007291}\chi_{UVA}\chi_{PYR} \\
& + 0.008186\chi_{UVA}\chi_{ALM} + 0.008582\chi_{UVA}\chi_{GRO} \\
& + {-0.002503}\chi_{PYR}{}^2\chi_{ALM} - 0.006987\chi_{PYR}{}^2\chi_{GRO} \\
& - 0.003973\chi_{ALM}{}^2\chi_{PYR} + {+0.006750}\chi_{ALM}{}^2\chi_{GRO} \\
& - 0.001263\chi_{GRO}{}^2\chi_{PYR} + 0.004874\chi_{GRO}{}^2\chi_{ALM} \\
& + {+0.032997} \pm 0.00007
\end{aligned} \tag{2}
$$

$$
\begin{aligned}
y(O) =\ & {-0.001239}\chi_{ALM} - 0.005065\chi_{GRO} - 0.028108\chi_{UVA} \\
& + {+0.009479}\chi_{PYR}\chi_{ALM} - 0.017111\chi_{PYR}\chi_{GRO} \\
& + 0.002962\chi_{GRO}\chi_{ALM} + {+0.026922}\chi_{UVA}\chi_{PYR} \\
& - 0.010858\chi_{UVA}\chi_{ALM} + 0.068324\chi_{UVA}\chi_{GRO} \\
& + {-0.008823}\chi_{PYR}{}^2\chi_{ALM} + 0.011940\chi_{PYR}{}^2\chi_{GRO} \\
& - 0.010982\chi_{ALM}{}^2\chi_{PYR} + {-0.005409}\chi_{ALM}{}^2\chi_{GRO} \\
& + 0.013992\chi_{GRO}{}^2\chi_{PYR} - 0.007035\chi_{GRO}{}^2\chi_{ALM} \\
& + {+0.050303} \pm 0.00008
\end{aligned} \tag{3}
$$

$$
\begin{aligned}
z(O) =\ & {-0.000408}\chi_{ALM} - 0.002016\chi_{GRO} + 0.011527\chi_{UVA} \\
& + {-0.013323}\chi_{PYR}\chi_{ALM} + 0.005439\chi_{PYR}\chi_{GRO} \\
& + 0.008104\chi_{GRO}\chi_{ALM} + {-0.011533}\chi_{UVA}\chi_{PYR} \\
& - 0.010870\chi_{UVA}\chi_{ALM} - 0.014516\chi_{UVA}\chi_{GRO} \\
& + {+0.013325}\chi_{PYR}^2\chi_{ALM} - 0.003669\chi_{PYR}{}^2\chi_{GRO} \\
& + 0.013530\chi_{ALM}{}^2\chi_{PYR} + {-0.006787}\chi_{ALM}{}^2\chi_{GRO} \\
& - 0.005797\chi_{GRO}{}^2\chi_{PYR} - 0.009530\chi_{GRO}{}^2\chi_{ALM} \\
& + 0.653287 \pm 0.00007
\end{aligned} \tag{4}
$$

under the constraint on the molar fractions of:

$$
\sum c = 1. \tag{5}
$$

The mole fractions of the end-members in our sample were then calculated by essentially inverting Equations (1)–(4) subject to the constraint given by (5). In practice this is achieved by adjusting the mole fractions using a least-squares procedure so as to minimize the squared differences between the observed values of cell edge, $x(O)$, $y(O)$ and $z(O)$ and those calculated by means of the right-hand sides of the Equations (1)–(4), respectively.

The resulting composition expressed as end-member mole fractions is:

$$Pyr_{0.41(5)}Alm_{0.36(7)}Gro_{0.22(1)}Uva_{0.01(1)}.$$
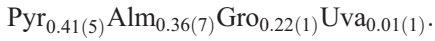
From the end-member fractions we can calculate the following chemical formula in atoms (the esd's in parentheses were obtained from the error propagation):

$$\left[Mg_{1.23(15)}Fe_{1.09(21)}Ca_{0.68(4)}\right]\left[Al_{1.98(17)}Cr_{0.02(2)}\right]Si_3O_{12}$$
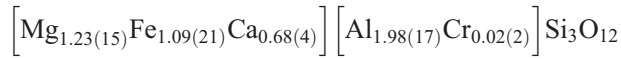
Some selected figures of merit related to the fitting of the original data are reported in Table 2. The large F-test values together with the small *p*-values related to the F-test allow us to reject the null hypothesis that the regression coefficients are zero, and can be considered as an evaluation of the goodness of the regression. Note that the evaluation of the F-test also allowed us to choose among some different models with different choices of the interaction parameters. As a further test of the reliability of model, the fractional coordinates and unit-cell parameter can be back-calculated from the derived composition through the Equations (1)–(4). Both the fractional coordinates and the bond lengths calculated in this way agree to within 1 *esd* with the values obtained from the structure refinement (Table 3).

All the standard deviations were calculated neglecting the covariance between the errors (*i.e.*, assuming that the errors are uncorrelated) using the usual error propagation formula. Note that (i) the errors associated to the geometrical parameters are those obtained for error propagation approach of the Equations (1)–(4) in which the variables are the end-member fractions and the Margules parameters, and (ii) the errors associated to the bond lengths are those obtained for error propagation approach of the Equations (6)–(9)) in which the variables are *a*, *x*, *y*, *z* and their associated uncertainties are those obtained in (i).

Effect of residual pressure on estimated garnet composition

Since the structure-composition model described above is based on X-ray diffraction data obtained from garnet crystals at room conditions, it cannot be directly applied to inclusions under significant residual pressure without considering the pressure effect on the unit cell parameters and the structure. Many mineral inclusions in diamonds, including garnet, however, are characterised by thermoelastic properties that result in very low or no residual pressures after the diamond is brought to Earth's surface. For example, Harris *et al.* (1970) measured the change of lattice parameters of two garnet inclusions in diamond by X-ray diffraction, first with the inclusions *in situ* and then freed from their hosts, and estimated 0.2 GPa remnant pressures on the inclusions. Cohen & Rosenfeld (1979) and Liu *et al.* (1990) studied five garnet inclusions in a single diamond from the Argyle mine (Western Australia) by microRaman spectroscopy. The spectra of all Argyle garnets indicated no internal pressure with an uncertainty

of about 0.25 GPa due to the low resolution (1 cm^{-1}) of the instrument used. Izraeli *et al.* (1999) carried out microRaman measurements of three diamonds containing peridotitic garnets close to the diamond-inclusion interface, and estimated internal pressures of 0.00–0.35 GPa. Such low internal pressures would have very little effect on the structural parameters (atomic coordinates and unit-cell edge) of the rigid crystal structure of garnet (*cf.* Zhang *et al.*, 1998) and therefore on their estimated chemical compositions.

A very cautious assessment of the potential bias on estimates of garnet chemical composition obtained with the procedure we employed can be made by (i) assuming that our garnet is under an internal pressure of 1 GPa (*i.e.*, much greater than reported in the literature for garnets trapped in diamonds) and (ii) extrapolating the geometrical parameters of the garnet to room pressure using known *P-V* equations of state for the different garnet end-members. Interpolation of Zhang's *et al.* (1998) data for pure pyrope to 1 GPa shows that the oxygen atomic coordinates *x* and *z* remain virtually unchanged, whereas the *y* coordinate increases by only 0.0006, *i.e.*, well below uncertainties of measurements based on X-ray diffraction. This value should approximately correspond to the predicted change for a pressure variation from 1 GPa to room conditions. The crystal structures of almandine and grossular are even more rigid than that of pyrope (Zhang *et al.*, 1999), therefore the above value represents an upper limit for pyrope-rich garnets. The corresponding change in the unit-cell edge can be calculated from the known *P-V* equations of state for the three main garnet end-members ($K_{T0} = 171$ GPa and $K' = 4.4$ for pyrope, $K_{T0} = 185$ GPa and $K' = 4.2$ for almandine, and $K_{T0} = 175$ GPa and $K' = 4.4$ for grossular). For the Jericho garnet composition, we estimated the equation-of-state parameters by linear interpolation of the end-member equations and obtained $K_{T0} \sim 175.2$ GPa and $K' \sim 4.3$. Using this equation of state, we can predict an increase of 0.0218 Å for the unit-cell edge of our garnet from 1 GPa to room pressure: from 11.5826 Å (if the garnet is supposed to be at 1 GPa) to 11.6044 Å at

Table 2. Some figures of merit related to the fitting of the garnet geometrical parameters by means of Equations (1)–(5) (see text). R = correlation coefficient; R^2 = R-Square statistics; SSE = Errors Sum of Squares; RMS = root mean square error; F = F statistics value; pval = *p*-value for the F statistics.

|	Uncorrected data	Corrected data
R	1.0000	1.0000
R^2	1.0000	1.0000
SSE	4.6312E–7	7.8084E–8
RMS	6.8053E–4	2.7943E–4
F	6.9562E+7	1.2871E+9
pval	8.8138E–5	1.7748E–5

Note: ''Uncorrected data'' refer to the actual inclusion *in situ* in the diamond host, and thus under residual pressure. ''Corrected data'' have been corrected for the possible effects of a residual pressure of 1 GPa.

Table 3. Observed and calculated structural parameters of garnet.

Geometrical parameters	Uncorrected data		Corrected data	
	Observed	Calculated	Observed	Calculated
Unit-cell edge a (Å)	11.5826 (2)	11.583 (18)	11.6044 (2)	11.605 (29)
Oxygen coordinates				
x(O)	0.0346 (2)	0.0343 (6)	0.0346 (2)	0.0344 (6)
y(O)	0.0484 (2)	0.0482 (3)	0.0478 (2)	0.0481 (4)
z(O)	0.6527 (2)	0.6528 (1)	0.6527 (2)	0.6527 (1)
Bond lengths (Å)				
Z-O($\times$4)	1.638 (2)	1.638 (5)	1.638 (2)	1.641 (7)
Y-O($\times$6)	1.898 (2)	1.898 (3)	1.899 (2)	1.900 (5)
X1-O($\times$4)	2.237 (2)	2.233 (6)	2.239 (2)	2.237 (8)
X2-O($\times$4)	2.391 (2)	2.393 (5)	2.402 (2)	2.398 (8)

Note: ''Uncorrected data'' refer to the actual inclusion *in situ* in the diamond host, and thus under residual pressure. ''Corrected data'' have been corrected for the possible effects of a residual pressure of 1 GPa. ''Observed'' are parameters obtained by experiment and structure refinement, ''Calculated'' from the Margules model of garnet structure.

room pressure. Using the modified values for O(y) increased by 0.0006 and a unit-cell edge = 11.5826 Å + 0.0218 Å = 11.6044 Å we obtain the following end-members fractions: $Pyr_{0.39(4)}Alm_{0.35(4)}Gro_{0.24(5)}Uva_{0.02(1)}$, which corresponds to the chemical formula (as above the esd's, reported in parentheses, were obtained from the error propagation):

$$\left[Mg_{1.17(12)}Fe_{1.05(12)}Ca_{0.78(15)}\right]\left[Al_{1.96(15)}Cr_{0.04(2)}\right]Si_3O_{12}.$$
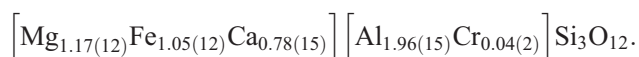
The results are within the uncertainties of those obtained using the measured geometrical parameters. We conclude that for typical garnet inclusions in diamond, the effect of remnant pressure on chemical compositions estimated with our method is minimal.

Discussion and concluding remarks

In this work we reported the crystal structure of a garnet inclusion enclosed in a diamond, as determined by means of single-crystal X-ray diffraction. The experimental procedure was previously applied in high-pressure crystallographic studies using diamond anvil cells and on a single olivine inclusion in diamond (Nestola *et al.*, 2011). The structure data, together with the formulation of an improved structure-composition model for garnet (according to Merli *et al.*, 1995) and the very reasonable assumption that the garnet is under relatively low internal pressure (below 1 GPa), allowed us to estimate the chemical composition as, expressed as end-member fractions, $Pyr_{0.41(5)}Alm_{0.36(7)}Gro_{0.22(1)}Uva_{0.01(1)}$. Uncertainties are higher than for a conventional electron microprobe

analysis, but sufficiently small for a precise classification of the garnet and thus broad petrological purposes, without having to destroy the inclusion as would be required by conventional chemical analysis. The estimated composition is typical of a low-Cr eclogitic garnet and lies within the field of the most common garnet inclusions in diamonds from the Jericho kimberlite (''eclogitic'' 90 %, ''websteritic'' 7 %, ''peridotitic'' 3 %; De Stefano *et al.*, 2009). The use of a complementary technique such as X-ray computed micro-tomography, allowed us not only to determine the size of both inclusion and diamond, as well as the exact position of the inclusion in the diamond, but also to find several smaller inclusions, which were not detected by optical examination. Among these, we could identify a second inclusion with similar X-ray absorption as the large garnet, probably a second garnet with similar composition, and some other smaller inclusions that require further work to completely characterise.

Our experimental approach demonstrates that it is possible to obtain crystal structure and chemical information on inclusions fully enclosed in their host diamond even when the inclusion is hardly visible under an optical microscope and when the mineral inclusion is chemically heterogeneous in terms of number of cation substitutions. We envisage that our approach can be extended to study a wide variety of mineral inclusions in diamond showing complex chemistry and crystal structure, provided a comprehensive crystallographic database of end-member and intermediate compositions and reliable equations of state are available.

References

Abramoff, M.D., Magelhaes, P.J., Ram, S.J. (2004): Image processing with ImageJ. *Biophotonics Int.*, **11**, 36–42.

Angel, R.J. & Finger, L.W. (2011): SINGLE: a program to control single-crystal diffractometers. *J. Appl. Crystallogr.*, **44**, 247–251.

Angel, R.J., Allan, D.R., Miletich, R., Finger, L.W. (1997): The use of quartz as an internal pressure standard in high pressure crystallography. *J. Appl. Crystallogr.*, **30**, 461–466.

Angel, R.J., Downs, R.T., Finger, L.W. (2000): *in* ''High-temperature and high-pressure crystal chemistry'',R.M. Hazen, R.T. Downs, eds., *Rev. Mineral. Geochem.*, **41**, Mineralogical Society of America and Geochemical Society, Washington, DC, 559–596.

Barron, L.M., Barron, B.J., Mernagh, T.P., Birch, W.D. (2008): Ultrahigh pressure macro diamonds from Copeton (New South Wales, Australia), based on Raman spectroscopy of inclusions. *Ore Geol. Rev.*, **34**, 76–86.

Brenker, F.E., Vincze, L., Vekemans, B., Nasdala, L., Stachel, T., Vollmer, C., Kersten, M., Somogyi, A., Adams, F., Joswig, W.,

Harris, J.W. (2005): Detection of a Ca-rich lithology in the Earth's deep (> 300 km) convecting mantle. *Earth Planet. Sci. Lett.*, **236**, 579–587.

Cohen, L.H. & Rosenfeld, J.L. (1979): Diamond: depth of crystallization inferred from compressed included garnet. *J. Geol.*, **87**, 333–340.

De Stefano, A., Kopylova, M., Cartigny, P., Afanasiev, V. (2009): Diamonds and eclogites of the Jericho kimberlite (Northern Canada). *Contrib. Mineral. Petrol.*, **158**, 295–315.

Feldkamp, L.A., Davis, L.C., Kress, J.W. (1984): Practical cone-beam algorithm, *J. Opt. Soc. Am.*, **A1**, 612–619.

Harris, J.W., Milledge, H.J., Barron, T.H.K., Munn, R.W. (1970): Thermal expansion of garnet included in diamond. *J. Geophys. Res.*, **75**, 5775–5792.

Izraeli, E.S., Harris, J.W., Navon, O. (1999): Raman barometry of diamond formation. *Earth Planet. Sci. Lett.*, **173**, 351–360.

Joswig, W. (2011): In situ X-ray diffraction investigations of a multiphase inclusion in a diamond from the Juina district, Brazil. *Z. Kristallogr.*, **226**, 226–228.

Kak, A.C. & Slaney, M. (1988): Principles of computerized tomographic imaging. IEEE Press, New York, NY.

King, H.E. & Finger, L. (1979): Diffracted beam crystal centering and its application to high pressure crystallography. *J. Appl. Crystallogr.*, **12**, 374–378.

Kunz, M., Gillet, P., Fiquet, G., Sautter, V., Graafsma, H., Conrad, P., Harris, J.W. (2002): Combined in situ X-ray diffraction and Raman spectroscopy on majoritic garnet inclusions in diamonds. *Earth Planet Sci. Lett.*, **198**, 485–493.

Liu, L.G., Mernagh, T.P., Jaques, A.L. (1990): A mineralogical Raman spectroscopy study on eclogitic garnet inclusions in diamonds from Argyle. *Contrib. Mineral. Petrol.*, **105**, 156–161.

Merli, M., Callegari, A., Cannillo, E., Caucia, F., Leona, M., Oberti, R., Ungaretti, L. (1995): Crystal-chemical complexity in natural garnets: structural constraints on chemical variability. *Eur. J. Mineral.*, **7**, 1239–1249.

Nestola, F., Boffa Ballaran, T., Tribaudino, M., Ohashi, H. (2005): Compressional behaviour of $CaNiSi_2O_6$ clinopyroxene: bulk modulus systematic and cation type in clinopyroxenes. *Phys. Chem. Minerals*, **32**, 222–227.

Nestola, F., Boffa Ballaran, T., Liebske C., Thompson R., Downs, R.T. (2008): The effect of the hedenbergitic substitution on the compressibility of jadeite. *Am. Mineral.*, **93**, 1005–1013.

Nestola, F., Nimis, P., Ziberna, L., Longo, M., Marzoli, A., Harris, J.W., Manghnani, M.H., Fedortchouk, Y. (2011): First crystal-structure determination of olivine in diamond: composition and implications for provenance in the Earth's mantle. *Earth Planet. Sci. Lett.*, **305**, 249–255.

Ralph, R.L. & Finger, L.W. (1982): A computer program for refinement of crystal orientation matrix and lattice constants from diffractometer data with lattice symmetry constraints. *J. Appl. Crystallogr.*, **15**, 537–539.

Sheldrick, G.M. (2008): A short history of SHELX. *Acta Crystallogr.*, **A64**:112–122.

Sijbers, J. & Postnov, A. (2004): Reduction of ring artefacts in high resolution micro-CT reconstructions. *Phys. Med. Biol.*, **49**, 247–253.

Sitepu, H., Kopylova, M.G., Quirt, D.H., Cutler, J.N., Kotzer, T.G. (2005): Synchrotron micro-X-ray fluorescence analysis of natural diamonds: first steps in identification of mineral inclusions in situ. *Am. Mineral.*, **90**, 1740–1747.

Smith, E.M., Kopylova M.G., Dubrovinsky L., Navon, O., Ryder, J., Tomlinson, E.L. (2011): Transmission X-ray diffraction as a new tool for diamond fluid inclusion studies. *Mineral. Mag.*, **75**, 2657–2675.

Stachel, T. & Harris, J.W. (2008): The origin of cratonic diamonds – constraints from mineral inclusions. *Ore Geol. Rev.*, **34**, 5–32.

Stoe, and Cie (1999): Crystal optimisation for numerical absorption correction. Stoe and Cie GmbH, Darmstadt.

— (2001): Data reduction program. Stoe and Cie GmbH, Darmstadt.

Wilkins, S.W., Gureyev, T.E., Gao, D., Pogany, A., Stevenson, A.W. (1996): Phase-contrast imaging using polychromatic hard X-rays. *Nature*, **384**, 335–338.

Zhang, L., Ahsbashs, H., Kutoglu, A. (1998): Hydrostatic compression and crystal structure of pyrope to 33 GPa. *Phys. Chem. Minerals*, **25**, 301–307.

Zhang, L., Ahsbashs, H., Kutoglu, A., Geiger, C.A. (1999): Single-crystal hydrostatic compression of synthetic pyrope, almandine, spessartine, grossular and andradite garnets at high pressures. *Phys. Chem. Minerals*, **27**, 52–58.

Yasuzuka, T., Ishibashi, H., Arakawa, M., Yamamoto, J., Kagi, H. (2009): Simultaneous determination of Mg# and residual pressure in olivine using micro-Raman spectroscopy. *J. Mineral. Petrol. Sci.*, **104**, 395–400.